On stability and relaxation techniques for partitioned fluid-structure interaction simulations.

PhD Student J. Lorentzon[a,*], Prof. J. Revstedt[b]

[a]Department of Theoretical Chemistry, Lund University, P.O. Box 124, 221 00 Lund, Sweden
[b]Department of Energy Sciences, LTH, Lund University, P.O. Box 118, 221 00 Lund, Sweden

ARTICLE INFO

Keywords:
LES
FSI
Partitioned
Stability
Relaxation

ABSTRACT

The stability of relaxation techniques has been studied for strongly coupled fluid-structure interaction (FSI) with application to a cantilever immersed in channel flow. The fluid is governed by Navier-Stokes equations for incompressible flow condition using turbulence modelling and the solid is governed by the equation of motion with compressible material modelling. The applied kinematic description is Lagrangian for the solid and Eulerian for the fluid. The coupling of the state solvers is achieved by the Arbitrary Lagrange-Euler procedure which involves a mesh motion solver and the FSI procedure is stabilised by relaxation. It is shown that the stability can be related to the frequency shift caused by FSI and they follow the same rate for the shape factor of the structure with an offset. This correlates well to theoretical results but also show that for given mesh resolution, all relaxations fail for sufficient high-frequency shift. We also propose a continuation technique to stabilise the solution near the instability region, which also improves the efficiency and can be integrated easily for the black-box FSI solution procedure.

1. Introduction

Recent developments in fluid-structure interaction (FSI), see[1, 2, 3, 4, 5, 6, 7, 8] and references therein, are focused upon algorithms that allows for a partitioned approach, such as interfaced Newton-Krylov techniques [1, 7, 8], rather than monolithic techniques [9, 10, 11, 12]. There is a strong incitement for using a coupling technique that allows two established solvers to be merged into a multi-physics solver. The subject of stability [13, 14, 15, 16, 17, 18, 19, 20] and performance on partition techniques have been thoroughly investigated during the last decade for numerous different blocked Gauss-Seidel (BGS) procedures using the Dirichlet-Neumann exchange procedure (DN) across the coupled boundary, with the source of instability as the interfering "low" frequency energetic modes in the flexuration of the structure [13, 21]. From several of the already mentioned articles on the subject of stability, it is clear that a large number of sources affect stability. Firstly, in the discretisation of the governing equations, the choice of numerical schemes and time step strongly affect the stability, the higher order of accuracy and shorter time step lowers the stability. Applied constraints influence as well, for example, the incompressibility assumption, increases instability. Further, the mass ratio between fluid and solid, material properties, form factors of structure and fluid domain, boundary conditions, all influences stability. Several of these are of course interrelated. It is therefore almost an impossible task to present a unified picture of the stability and its parameter dependency, but for incompressible solvers in linearisable case settings, for sufficiently small time step, there are mainly two parameters that affect the stability, the mass ratio and a structural factor that is a function of the form factor of the structure and the eigenvalue of the added mass operator.

A closed expression for stability condition, a criterion that gives an apriori knowledge of the feasibility of an FSI methodology, is unattainable for three-dimensional Navier stokes equations (NS). There are however theoretical studies for simplified cases that exist, such as von Neumann analysis applied to one-dimensional problems. One of the most common such applied cases in FSI is the two-dimensional channel flow with thin flexible membrane allowing a one-dimensional FSI formulation, using linearised governing equations, which provides a stability criterion for the fixed-point iteration and its successive-under-relaxation technique (SUR) of the BGS procedure[3, 21, 22, 23, 24, 25, 26]. These show that in incompressible flow, for sufficiently small time steps, only the mass ratio and a structural factor, determines the stability for the DN exchange procedure and that for compressible flow, for sufficiently small time step, the FSI methodology is stable. Another problem leading to the same conclusion is the piston problem [19, 27]. Also,

*Corresponding author
johan.lorentzon@teokem.lu.se (J. Lorentzon); johan.revstedt@energy.lth.se (J. Revstedt)
ORCID(s): 0000-0002-3596-2483 (J. Lorentzon); 0000-0003-3215-3098 (J. Revstedt)

the stabilisation techniques such as IGMRES, Aitken δ^2 and SUR have been analysed [28] for a beam in coupling with a uniform flow, providing a detailed description of stability and efficiency in terms of eigenmodes as a function of coupling iteration and its dependency on the mode-dependent mass-ratio. Although these analyses are useful in providing criteria for stability, their limitation to linear problems may be an issue [16] and may even make them infeasible in evaluating the criteria for some relaxation procedures such as the residual techniques. Also, it is desirable to achieve criteria that can be related to design parameters. For that reason, one often complement such studies with benchmark/validation cases, involving two/three-dimensional cases [21].

The incentive of this study comes from two major observations. Firstly, in the literature, there is no empirical comparison of stability criteria for FSI methodologies applied to fully three dimensional Navier-Stokes equations. Instead, there are only studies of efficiency in comparison such as the pioneering work by Vienderals [2] on quasi-newton methods that preluded the works of Degroote et al [27], where the IQN-ILS were investigated for FSI problems, Küttler et al [7] proposing Aitken δ^2 and so forth. One such commonly applied case is the pressure pulse velocity driven three-dimensional elastic tube, which by using settings from [27], produced biased results in our investigation such that it was near instability for a strongly coupled FSI without relaxation and the Aitken δ^2 method was impaired by its sensitivity to noise that was accentuated by the settings. Despite this, the efficiency matched the published results well. This raises several questions, such as if the pressure response was critical in the analysis of the results, it is very seldom such data are available. We, therefore, question the reproducibility of this case with the settings presented. Secondly, the (DN) exchange procedure is challenged when a solid solver is coupled with an incompressible fluid solver. This is accentuated while using a compressible solid solver applied to nearly incompressible solid, i.e. approaching a Poisson ratio of 0.5, for issues like "locking" and nonproportional pressure response arise. While there exist, solid solvers that handle this issue, such as finite volume approaches[29], these are mainly useful when using a monolithic approach and will not resolve the issue for a partitioned approach. The cause for this issue is that any size of displacement in the solid solution vector with high-frequency components, with a numerical error or physical origin, induces a large pressure response from the fluid solver and while applying this to an immersed body, or more precisely, when the fluid compresses the solid due to the design of the application, will trigger spurious evolutions of the compression waves. With stabilisation, these waves can be suppressed but whenever the response by compression is coupled with the excitation, the problem most likely requires a compressible flow solver, otherwise the results may be inaccurate.

These above issues can be avoided by the design of the application, proper choice of discretisation, material setting (Poisson ratio) or by using suppression. For example, thin-wall/slender structures[1], proper time step/spatial resolution[2], or implicit damping/filtering[3]. This is a well-known issue and can be motivated as long as preserving the accuracy holds over efficiency/stability. The FSI instability of a partitioned methodology with DN exchange is associated with partition error, larger the instability, the larger the partition error, creating three different types of failures of the FSI methodology, namely, cell distortion in the mesh for the ALE description, failure in coupling across of the interface, where the solid solver diverges by the overpressure response from the fluid, and the failure in resolving the low amplitude residues that growths over time and triggers overpressure failure. In most analyses of the stability, the growth factor of the error, the focus is on the low amplitude, since it is primary that aspect that set the stability limit for the FSI coupling. Despite that overpressure and low amplitude residues have a common source, the growth factor of the error, the way it occurs, affects the interpretation of methodology, some relaxations are more effective towards suppressing overpressure, others more effective in resolving low amplitude residue.

Another issue often overseen is the conditionality of the solution matrix, most studies of stability criteria are limited by coarse resolution applied upon fairly easy complied FSI problems. This leads to well-posed problems with very limited possibility to validate against issues that often challenge the FSI procedure when the traction across the coupled boundary contains high-frequency small-scaled motion, for example, turbulence.

A suitable test case should strongly challenge the FSI methodology but also be feasible and reproducible, possible to evaluate experimentally and be related to some engineering application. In our pursuit of a suitable test case we have evaluated several applications containing turbulent flow, such as the splitter blade behind a bluff body, thin

[1] The Poisson ratio generally does not influence the stability for a stand-alone solid-state application of a cantilever, this is due to the aspect ratio/thickness, as described in [30] on page 369. However, there is to our knowledge in the literature no study of the dependency of the Poisson ratio (i.e. speed of sound in solid) for an FSI application with an incompressible fluid, an overseen feature.

[2] Most compression and high-frequency components have a low amplitude, so by coarse resolution over the solid and time step, these components are not captured across the interface more than aliasing and then becoming of negligible influence, however, by increased resolution, these can be resolved, may affect both stability limits and conditionality

[3] By applying filtering/POD across the interface only, high-frequency but low amplitude fluctuations can be removed, thus resulting in separation of scales between low amplitude high-frequency content in residuals and the low-frequency amplitudes of the solution vector

beam/cantilever acting as a bluff body [31], elastic tubes [32], channel flow [33], using either a free-stream/pulsating flow or still tank. We found that the vortex-induced vibrations on a finite length cantilever immersed in a channel flow are a well-suited case for the FSI challenge, reproducibility and feasibility. Also, the availability of theoretical results from beam theory and inviscid flow is considered as an advantage. The mesh/domain of the channel flow case is chosen with the intention that it can be used as a benchmark case, i.e. with a mesh of a few million cells one can get a solution in about 24 hours on a high-performance desktop PC (e.g. with Xeon processors) using about 20 cores.

The primary goal in this study is to establish the stability criteria for the most commonly applied relaxations in FSI reported in the literature: SUR[34], Aitkens δ^2 method [7] and IQN-ILS [1]. The FSI methodology applied is the BGS procedure with (DN) exchange across the coupled boundary that implicitly resolves the issue of low amplitude residues that is recently published [35]. We will present a characterisation of the FSI with stability criteria for each mentioned stabilisation method and the mechanism of the failure in the FSI black-box procedure will be analysed by studying the norm of the residuals as a function of the subiteration index. We also present a hybrid technique with homotopy, although applied to IQN-ILS, but can be used with any relaxation, that improves the stability range for minimal impact of efficiency.

2. Methodology

In the following, the FSI procedure is shortly described together with the definitions of FSI conditions. Only details relevant to this study are explained, for more information about this methodology and validation see further in a previous study [35]. For each domain, the governing equations and algorithms for solving these are defined, the so-called solution step. The applied stabilisation procedures, in terms of continuation, relaxation and filtering procedures are stated in separate sections. Tensor notation is applied, where the derivatives are shown by appending a comma-separated index to the subscript, for example, $a_{i,j} \equiv \partial_j(a_i)$. The superscripts f and s used with state variables, refer to the fluid and solid sub-domains, respectively, but will be dropped whenever they are obvious from the context.

2.1. Problem description and boundary conditions

The balance equations applied are the conservation of mass and momentum. The domain is divided into a fluid and a solid subdomain, and each is further partitioned into cells, these define the mesh. Each cell has a set of boundary elements. where the common boundary, Γ between the domains is subjected to a Dirichlet-Neumann condition,

$$v_i^f = a_{i,t}^s \ , \ \ \sigma_{ij}^s n_j^s = -\sigma_{ij}^f n_j^f \ , \tag{1}$$

where v_i^f is the boundary velocity on the fluid domain side with a no-slip condition, a_i^s is the displacement vector of the structure, n_i is the normal vector to the face element for a given cell in the sub-domain and σ_{ij} is the Cauchy stress tensor. The traction on each boundary element is defined as $t_i = \sigma_{ij} n_j$. Each domain has its solution step, that solves the balance equations for given boundary conditions and initial conditions. The exchange of state variables over the coupled boundary can be expressed as a mapping $t_i = \mathcal{F}(a_i)$ for the traction, and likewise $a_i = \mathcal{S}(t_i)$ for the displacement. The condition for the coupled problem can then be reformulated as a composite mapping,

$$a_i = (\mathcal{S} \circ \mathcal{F})(a_i) \equiv \mathcal{H}(a_i) \tag{2}$$

where t_i is the traction and a_i is the displacement. This composite mapping of solution steps is henceforth referred to as the coupling procedure. Only these variables across the boundary, provided by the composite map, are accessible by both state solvers. Hence, it is a partitioned procedure and we are calling these fields as the interface field variables and in equation denoting them as a_i^*/t_i^*. The unknown displacement variable a_i is determined by a Blocked-Gauss-Seidel approach (BGS), a fixed point approach, for further details see [35]. Whenever no stabilisation is applied, the coupling procedure is referred to as the implicit procedure. The infinity norm of the displacement field from the solid step is applied as the end condition for the fixed-point iteration after the fluid step is performed. In all calculations, the fluid step is the most expensive part of the simulation.

2.2. Fluid step ($\mathcal{F}$)

The Fluid step is a composite map of a mesh motion solver and a fluid solver. The mesh motion solver computes the so-called relative velocity (U_i^r) and enforces the Geometric Laws of Constraints (GLC) to be satisfied. The fluid

solver provides a solution of the Incompressible Navier-Stokes equation (INS) which is expressed in strong form by the Arbitrary-Lagrange-Eulerian (ALE) description takes the following form,

$$U_{i,t} + U_j^r U_{i,j} - 2\nu D_{ij,j} = -\frac{1}{\rho_f} p_{,i} \,, \tag{3}$$

where U_i is the fluid parcel velocity, D_{ij} is the strain rate tensor, ν is the kinematic viscosity, and p, is the pressure. Turbulence is modelled by Large-Eddy-Simulation (LES), which in short can be formulated as adding an extra term (the subgrid scale tensor) which reflects the influence of the unresolved turbulent scales, for further details see [36]. The fluid and mesh solver are taken from the open-source package OpenFOAM [37].

2.3. Solid step ($\mathcal{S}$)

The governing equation for the solid is the equation of motion,

$$\rho_s a_{i,tt} - \sigma_{ij,j} = f_i^e, \tag{4}$$

where the σ_{ij} is the Cauchy stress tensor and f_i^e is the external force per unit volume. The semi-discretised form of the equation of motion, Eqn (4) can then be transformed into,

$$M_{ij} a_{j,tt} + C_{ij} a_{j,t} + F(a_i) = F_i^e(t), \tag{5}$$

where M_{ij} is the consistent mass matrix, C_{ij} is the damping matrix and $F(a_i)$ the internal force. The Rayleigh damping (RD) model defines the C_{ij} matrix as

$$C_{ij} = \alpha M_{ij} + \beta K_{ij}, \tag{6}$$

where K_{ij} is the stiffness matrix. The damping ratio ζ relates to the RD model as follows,

$$\zeta = \frac{\alpha}{2\omega} + \frac{\beta}{2}\omega \,, \tag{7}$$

where ω is the forcing frequency in steady state. The internal force $F(a_i)$ is computed by using finite strain theory from which the stiffness matrix is obtained, with hyperelastic approach in Total Lagrangian description. The linear Hookean material model is applied, involving the Young's modulus (E) and the Poisson ratio (ν_s) as material parameters. An energy conserving temporal discretisation algorithm is applied, using a Newmark procedure. The procedure implemented is proposed by Bathe[38] using deal.II library package [39].

2.4. Stabilisation techniques of the FSI coupling.

A simple but efficient way to invoke relaxation to fixed point solution to Eqn (2) is to blend the current solution step $k+1$ with the previous solution step k,

$$a_i^* = a_i^k(1-\omega) + \omega a_i^{k+1}, \tag{8}$$

where $a_i^{k+1} \equiv \mathcal{H}(a_i^k)$ and ω is a fixed parameter. Whenever $0 < \omega < 1$, this is called the successive-under-relaxation technique (SUR). To generalise this, the fixed-point iterative solution procedure of Eqn (2) can be reformulated into a residual form for given sub-iteration k,

$$r_i^k = \mathcal{H}(a_i^k) - a_i^k, \tag{9}$$

defining the solution for this problem for given time step n as a_i^n. Then by applying an approximate Newton method with Jacobian $J(a_i^0, .., a_i^k)$ with respect to Eqn (9) gives an update method,

$$a_i^* = a_i^k - J_{li}^{-1} r_l^k. \tag{10}$$

Hence, $a_i^k \to a_i^n$ as k increases. During each subiteration, the inverse Jacobian J_{li}^{-1} is implicitly evaluated by using a procedure known as the IQN-ILS(X) presented by Degroote et al [27], where X is the number of intermediate solutions steps a_i^l used in the LSQR procedure. This involves at least two iterations before applying it as a post-correction before

the mesh motion solver. By keeping the residuals of the corresponding subiteration from previous time steps, one can achieve improved efficiency, then successively replace them by the current time steps residuals, this is called IQN-ILS-R[4].

For X=3, the Aitken δ^2 method[5] [7], defines an optimised blending,

$$\omega^k = \omega^{k-1} \frac{(r^{k-1})^T (r^k - r^{k-1})}{(r^k - r^{k-1})^T (r^k - r^{k-1})}, \tag{11}$$

where $w^0 = 1$. This is generally an efficient procedure but for "noisy" data it can be unstable.

In the coming sections, we define the relative error as $\Delta_i^k = r_i^k / \delta a_i^n$, where $\delta a_i^n = a_i^n - a_i^{n-1}$ is the increment for given time step and $r_i^k = a_i^k - a_i^{k-1}$ is the residual for subiteration k. To improve the performance, the first step is normally estimated by extrapolation step[6].

2.5. Preconditioning: continuation

Blending is the simplest homotopy between two continuous functions g and f,

$$f^* = \omega g + (1 - \omega) f. \tag{12}$$

By continuously changing ω from 0 to 1, the function f^* continuously changes from f over to g. This is commonly applied when a solution f is known and the solution g for another but a similar problem is sought. Using the continuation technique, one can then move the solution in state space instead of solving the original full equation. In this study, we apply this by asserting the following equation of motion,

$$\omega^m M_{ij} a_{j,tt} + \omega^d C_{ij} a_{j,t} + \omega^k F(a_j) = (1 - \omega^t) F_i^e(t - \Delta t) + \omega^t F_i^e(t), \tag{13}$$

see [35] for more details. By assuming linear state solvers and linear material modelling, only the input parameters to the solid-state solver and the traction are thus altered, all stored in the interface. More specific, incremental loading of the traction (ω^t) as Eqn (12) prescribes with predicted/previous time step traction as the starting load and the current traction as the final load. A scaling function ω is assigned to the mass[7], the damping ratio and the stiffness. We are in this study referring ω^t as traction SUR, the application of the other three scaling parameters, i.e ($\omega^m, \omega^d, \omega^k$) is phrased as the continuation. The ω is parametrised as a function of predefined precondition steps k,

$$\omega(k) = \gamma_0 + \gamma_2 \gamma_1^k, \tag{14}$$

and defined in triples $[\gamma_0, \gamma_1, \gamma_2]$. For continuation, we set $\gamma_0 = 1$ and $\gamma_1 < 1$ and $\gamma_2 = x_i / x_f - 1$, where x_i is the initial value and x_f is the final value, hence, $x_i = \omega(0) x_f$. For traction SUR we apply $\gamma_0 = 0$, $\gamma_1 < 1$ and $\gamma_2 \leq 1$. The blending function can be chosen fairly freely, as long as its convergence is sufficiently slow.

2.6. Traction: Finite Impulse Response filtering (FIR)

The fluctuation of higher-order frequency response can be quenched by applying convolution filtering and is applied to the interface field variable t_i^* before the transfer of the traction from fluid to solid step. The chosen filter technique is Finite Impulse Response [41], which is a low pass filtering with a cut off frequency X which we specify as FIR [X]. This stabilises the coupling procedure and could also be applied when the frequencies that cause destabilisation are known a priori.

[4] Relaxation normally only deals with the solutions of the current step, and as the author of IQN-ILS-R often uses the phrase "reuse" of the previous timestep, that refers to the residuals of the previous time step, not the solution vector. Otherwise, it would be a merely ROM technique.

[5] The Aitken δ^2 procedure can be considered as a special case of IQN-ILS(3), $J_{ij} = \omega^{-1} \delta_{ij}$ [1].

[6] As pointed out by the authors of IQN-ILS [1], using extrapolation functions often counter-effect the efficiency of the FSI procedure except at the first step. This since the procedure relies on exact correlation $x^* \rightarrow \mathcal{H}(x^*)$, by replacing $\mathcal{H}(x^*)$ with an interpolated field gives false residuals that jeopardise the procedure.

[7] The numerical continuation is similar in effect as with fictitious mass and damping method [40], although they require an algorithmic change which is not a black-box approach.

2.7. Categorisation of FSI coupling failure

We apply an empirical classification of coupling failures in the discussion of stability issues. A stable solution is whenever the fixed point iteration for Eqn (2) contracts to a well-defined solution, however not necessarily the physically correct one. Whenever the FSI procedure fails to converge in the fixed-point iteration by providing an unbounded result, while each solver provides for its input within given tolerances converged results, is denoted as a type I failure. Otherwise, if convergence for FSI cannot be reached but still a bounded solution is obtained is referred to as type II failure. The final type of failure in the coupling procedure lies in the mesh motion solver. When cells deform, they sometimes become ill-shaped. We denote this as type III failure which is unrelated to the stability of a relaxation which is the focus of this study. With any of these failures triggered, the partition error grows.

3. Setup of simulations

This section defines the solver settings used for each solver and gives a description of the domain and the applied boundary conditions. The material constants are also defined for the fluid and the structure, as well as the procedure used for the sampling of the response data by using probe points.

3.1. FSI tolerance

It is not feasible to set the FSI tolerance at numerical precision as it is for the linear solvers. For that reason, it is important to perform an FSI tolerance study for each case. The maximum number of iterations is set to 100, a necessity when approaching the stability limit.[8] Varying the tolerance from 10^{-4} down to 10^{-9}, stable and accurate results are obtained already at 10^{-6}, that is, the deviation in FSI coupling is less than the FSI tolerance compared to the most accurate solution. However, to emphasise accuracy over efficiency we are setting the FSI tolerance to 10^{-8}.

3.2. Domain and mesh description

The fluid domain is a rectangular box, with two opposite faces open (normal to the x-direction) and the other four boundaries are closed walls. The openings are velocity driven inlet respectively pressure outlet. A uniform velocity at the inlet in X-direction is applied with a flow speed U_∞=3 m/s and advective condition at the outlet were specified. At the walls, no-slip conditions and zero-gradient for the pressure were imposed. Throughout this study, we keep the height (L) and the width (b) of the cantilever constant and vary only the thickness (t). The aspect ratio (AR) is the thickness to height ratio expressed as the quotient (L/t). The Z-direction is along the axial direction of the cantilever. The mesh distribution with outlined bounding surfaces for both cases is shown in Figure 1, where an outline of the domain and an XZ cut plane of the mesh distribution for the fluid domain is presented. The width of the cantilever is set to b≡D. The distance to the openings from the cantilever's surface is set to 10D while the distance to the side walls is set to 7.5D. The fluid domain was given an unstructured grid composed of tetrahedral cells. The mesh is defined by the number of fluid cells per D unit at the surface of the cantilever, in this study 20 cells / D. The cell sizes were then gradually increased as a function of distance to this surface as described in [35].

[8] In the stable range and with the current application, the IQN-ILS/Aitken δ^2 method performs almost equal with around 4-8 subiterations depending on cantilever configuration and R^*

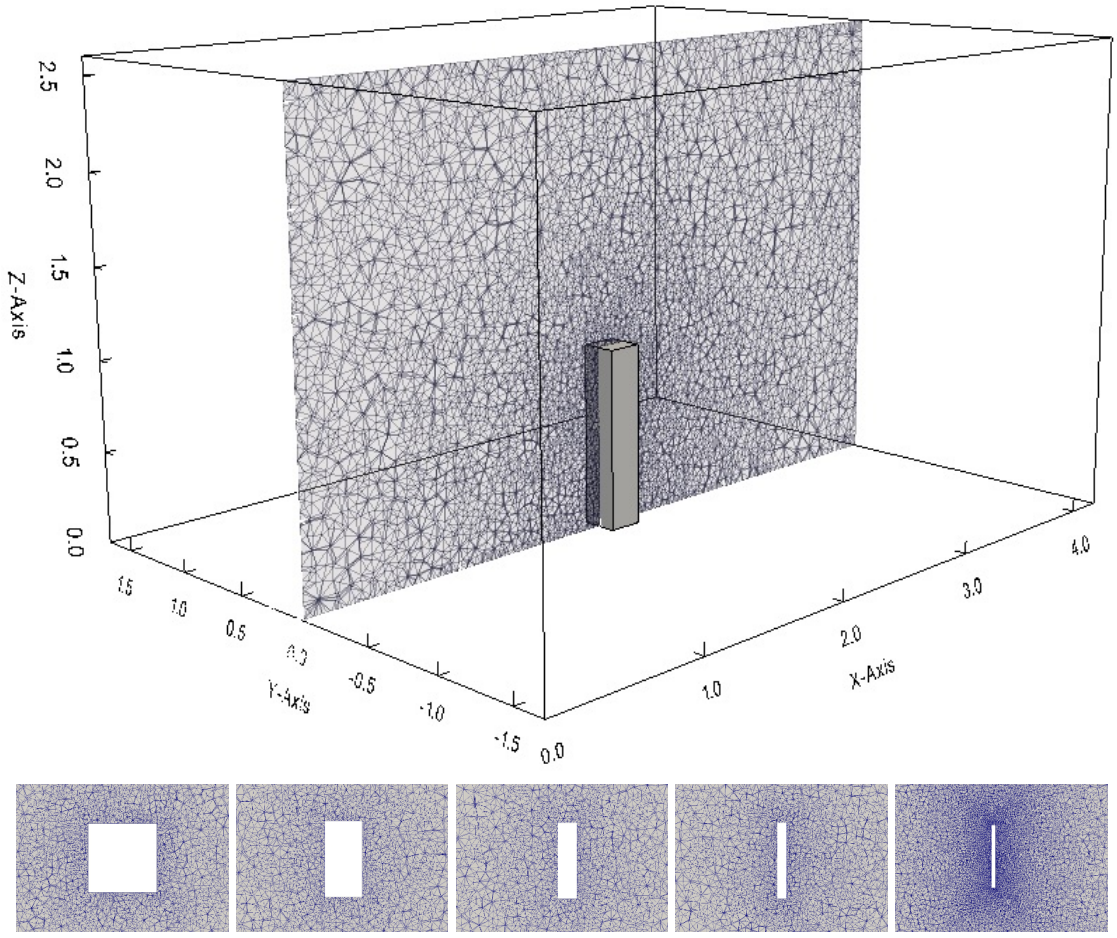

Figure 1: Upper: The fluid domain with two openings at ZY on X=0 and X=4 and solid walls on the rest. Cut plane in XZ through Y=0 shows the mesh distribution. Lower: The mesh distribution for different cross-sections in XY plane at Z=2.5D.

3.3. OpenFOAM solver settings

For the fluid step using OpenFOAM, the *pimpleDyMFoam* and the *displacementLaplacian* solver are used for the momentum and mesh motion mapping respectively. The discretisation schemes applied for the fluid solver are henceforth specified term-wise as in Eqn (3). For the divergence term, a Total Variation Diminishing (TVD) scheme is applied [42] and blended with an upwind scheme (0.1) for stability. For the spatial gradient terms, the central difference procedure with a limiter is applied. The time derivatives are discretised using the backward (BDF2) scheme [43]. As a sub-grid scale model in LES, the dynamic Smagorinsky is applied [44] which computes the average filtering by sampling over the whole domain in each direction, so-called *homogeneousDynSmagorinsky* model.

3.4. Material description

For the solid is mass density ρ_s (kg/m^3) which we vary for the study of the dependency in mass ratio, Young's modulus E= 58.8 MPa, and Poisson's ratio ν_s=0.3[9]. The damping ratio is $\zeta = 0$ unless otherwise stated. The fluid properties are density ρ_f=1000 kg/m^3. The mass ratio is defined as $R \equiv \rho_f/\rho_s$ and is varied by varying the density of the solid (ρ_s).

[9]The stability of the FSI procedure increases with increasing Poisson ratio, to the limit when the compressible solid solver reaches near incompressibility with $\nu_s \to 0.5$, the limitation occurs beyond 0.49 for current implementation and case setting, but of course, the error preludes already at lower values of ν_s but estimated from beam theory and high resolved grid, that error is less than 0.2% at Poisson ratio 0.47 for the current form factor.

3.5. Choice of Reynolds number

The cantilever Reynolds number ($Re = \frac{U_\infty b}{\nu}$) determines the flow characteristics and turbulence in the wake of the cantilever. With current settings, the Reynolds number should be in the range between 500 and 10000, beyond this interval, requires adjusted time stepping and increased mesh resolution, which biases the efficiency, although not stability. Since we are using fixed inlet bulk velocity[10], it is the kinematic viscosity (ν) that set the Reynolds number. The study was limited to the first few inline oscillations, hence no fully developed turbulent flow. The influence of the turbulence in this range and application on the FSI has shown to be negligible compared to the frontal pressure, the shear layer and the wake structure [35]. Further, the choice of domain is such as to keep the size of the high-resolution part of the mesh to a cost-efficient level. The removal of meshing for the vortex street is further motivated from a previous study [35] that shows without exception, the stability of the FSI procedure is determined during the transient phase, mostly due to the larger boundary velocity.

4. Results

The roadmap of this study is divided into several steps. First, we present a probe point analysis for the displacement of the cantilever. By analysing the forward derivatives of displacement at the probe point, we can visualise the convergence pattern in terms of the relative error for strongly coupled FSI. From this, we focus on the cause for the instability, the relative error and the high-frequency content in the third and fourth derivatives of the probe point data. The conclusion is that the true solution lies between two consecutive coupled iterations. For that reason, blending is a good choice. But knowing the blending is often difficult when the gain factor is large. We are presenting an alternative procedure, known as a continuation (outlined in Section 2.5) applied as a precondition. The stability of the method, together with other commonly applied relaxation techniques, is assessed by calculating the stability as a function of R and AR of the cantilever.

4.1. Causes of instability

To further characterise the FSI response, we now considering the probe point data at the centre of the tip of the cantilever for the channel flow case with $Re = 600$, R=1 and AR=5. First, we give an overview of the efficiency of the prediction/extrapolation, then we focus on the Taylor expansion of the displacement field, to identify important markers that characterise the FSI efficiency. Then we analyse the relative error and prediction, classify types of failures concerning efficiency and stability.

4.1.1. A stiff problem

We now analyse the flow for a simulation with no relaxation. Consider the displacement, shown in Figure 2 (left), where the largest response lies in the flow direction. The velocity field of the fluid at 0.6 s is presented in Figure 2 (right). The wake is building up but no vortex street has yet been formed.

[10]Our choice of boundary condition is based on the that we would like the flow impacting the cantilever to be as close to uniform as possible, i.e. keeping the boundary layer as thin as possible. A uniform inflow without turbulent fluctuations is then an obvious choice and that we find it reasonable to assume that such a condition is physically valid since it is regularly created in, for example, well-designed wind tunnels.

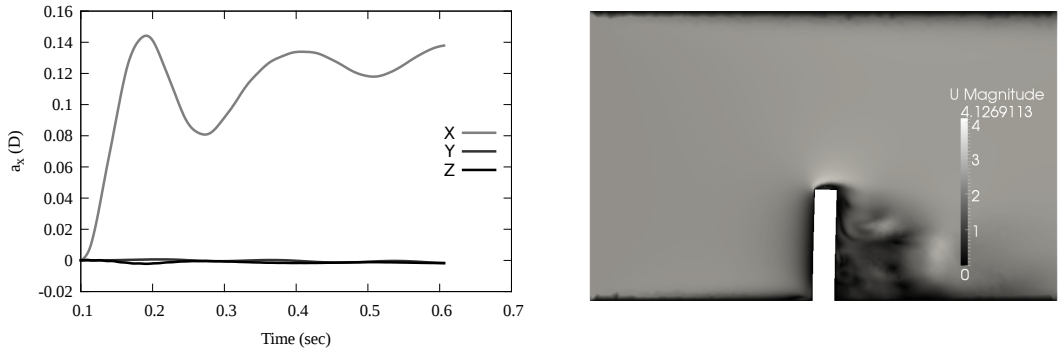

Figure 2: Left: Probe displacement data (X, Y, Z) components, X is in the flow direction, Z the axial direction. Right: Velocity profile at the mid-cut of the case.

The finite strain formulation with Newton's method has the evolution to next time step incorporated, where an estimator by first and second-order derivatives is used. This produces a significant proportion of stability in the FSI procedure. This can be seen in Figure 3 (left), where the increment in time step δa_i^n for probe displacement in the X-direction is displayed together with the residual after the first iteration (r_i^1). We denote *sgnlog* as the sign of Δ_x^k times the logarithm of the absolute value of Δ_x^k. Almost 98% of the displacement is reached by the first iteration and that is due to the estimator. As the FSI tolerance study shows, the FSI tolerance has to be 10^{-6} or smaller, since it is a stiff problem.

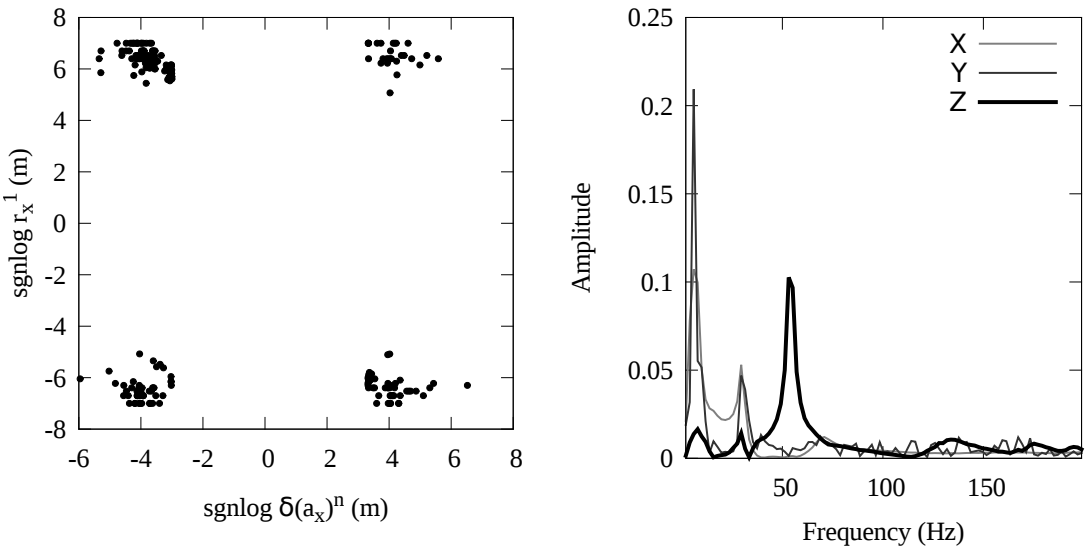

Figure 3: Left: correlation of δa_i^n, r_i^1 from Figure 2 in X direction. Right: Frequency distribution with amplitude distribution of δa_i^n.

The correlation between large scale motion and residuals ceases after the prediction step, shown in Figure 3 (left), where the subsequent sub iterations act more or less randomly. A Fourier analysis on the increment shows that it correlates strongly with bending modes (first and second) and compression wave along Z-axis in the cantilever, see Figure 3 (right). In other words, the prediction covers the larger-scale motion while the small scales requires further iterations until the precision is such as the small scales is sufficiently resolved.

4.1.2. Taylor expansion analysis: FSI efficiency in a nutshell

By using the displacement $a_i(t)$ at the probe point at the tip of the cantilever and taking the derivatives $\partial_t^n a_i$, one can compute Taylor terms for a given order ($f^{(n)} = \frac{1}{n!}\partial_t^n a_i \Delta t^n$). This is shown in Figure 4 in X-direction for implicit coupling up to the fourth-order by forward difference. An interesting feature is that the sum of the third and fourth-order terms is very close to the infinity norm of the residual for the first iteration, which verifies the accuracy in the prediction step during the first iteration.

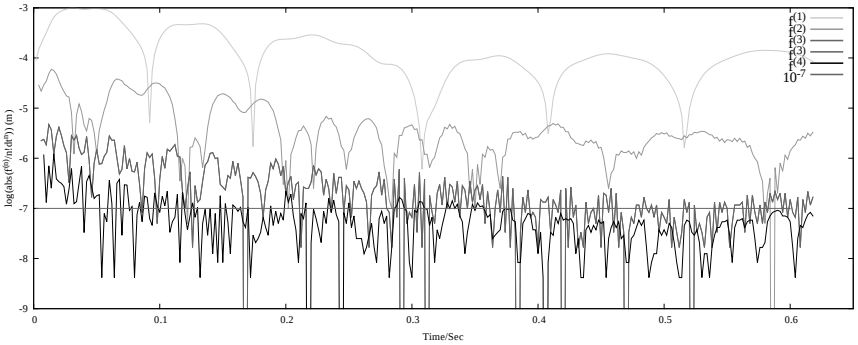

Figure 4: Taylor expansion term $f^{(n)} = \frac{1}{n!}\partial_t^n a_x \Delta t^n$ of probe point data, where the derivatives are estimated from a forward difference.

A general observation in the study of the Taylor expansion is that the efficiency of the FSI convergence is very much about the smoothness and the magnitude in derivatives with an order higher than one. The vast amount of third and fourth-order is due to the unloading of excess energy at the beginning of simulation that triggers multiple higher-order modes in the solid solver. Using a load ramp can significantly stabilise the simulation, but that is an unwanted feature in this study, we believe that the broad spectrum of frequencies is the main cause for that the stability limit that can be evaluated in the transient phase. Of course, the amount of third and fourth-order increases as cross-flow vibration starts, but not even at the synchronisation regime, the amount of third and fourth-order matches in size at beginning of the simulation.

4.1.3. Error analysis: The zig-zag response pattern

The relative error as a function of subiteration shows a zig-zag pattern that goes to zero, see Figure 5. Since the infinity norm is applied, the position may of course vary, however, the largest residual is normally located at the edges of the cantilever, closely corresponding to where the Courant number is highest. This is also the position where the pressure fluctuations is as largest on the surface of the cantilever. Figure 5 show the Δ_x^k, where the mean and standard deviation is computed from the in probe point at each macro step of corresponding subiteration k. The left panel depicts the zig-zag pattern of the mean value and the linear decrease in log scale for the standard deviation, while the right panel shows the exponential decay of the Δ_x^k. This is a behaviour we have observed for all simulations except when using the continuation technique or approaching in the vicinity of the stability limit of the FSI procedure. It is evident that the initial choice in fixed-point solution strongly affects the efficiency and also stability, a too large deviation may lead to an unbounded response, i.e. a type I failure. A study on FSI [17] using the BGS method, corroborates with this by depicting a similar pattern as described on the right panel, but the main focus in that study was on the blending technique and its sensitivity to optimisation, not the pattern itself.

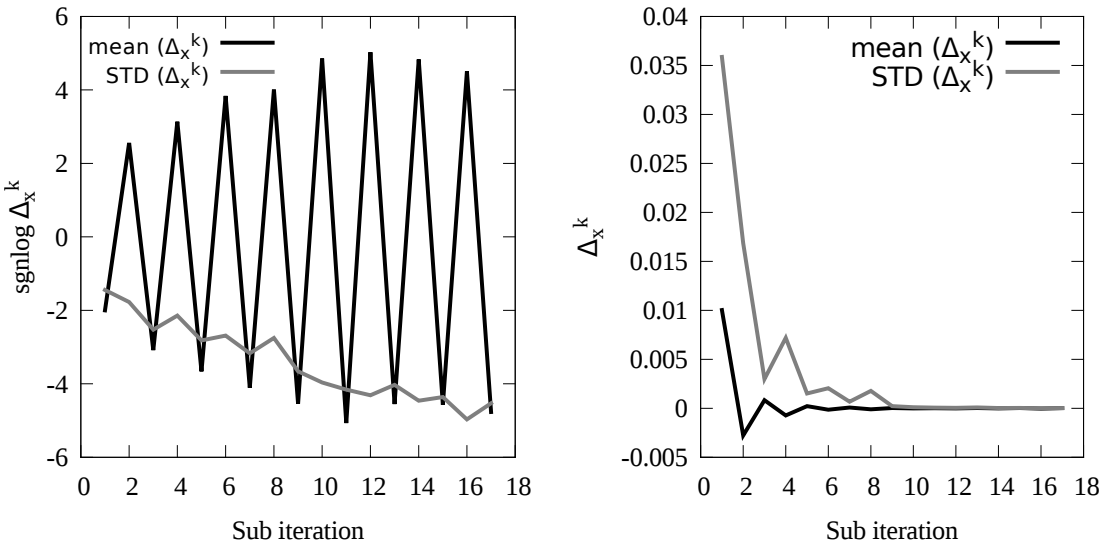

Figure 5: The mean and standard deviation of the relative error in the X-direction (Δ_x^k). Left: $sgn(\Delta_x^k)log(abs(\Delta_x^k))$ showing the zig-zag pattern. Right: Data of Δ_x^k showing the exponential decay

For a three-point stencil, providing an optimised blending, such as Aitken δ^2, the blending never exceeds 1 (over-relaxation) and it varies significantly as a function of sub iteration. The zig-zag pattern is reduced while applying under-relaxation ($\omega_k < 1$). The continuation technique also reduces this zig-zag or even eliminates it, depending on the choice of scaling factors. This often comes at a severe cost: it is more computationally intensive in terms of the number of subiterations.

4.1.4. Classification of instability

We choose a time step that minimises the spurious force response at the turning point caused by the mesh motion solver [35]. Further, we avoid too large deflection which otherwise would compromise the quality of the cells. Hence, by keeping a sufficiently low Courant number (average 0.2) and deformation less than 50% of the height, the type III failure is eliminated. Type I failure occurs whenever the zig-zag response pattern becomes unbounded and as result creating an artefact pressure response. This error thus often appears early in the simulation. Type II failure occurs whenever the infinity norm reaches the level of third and fourth derivative, but cannot resolve below that. The origin of this is twofold, firstly, the quality of the mesh and the settings of the thresholds for the fluid solver both affect the interpolation error. Secondly, the reverberation of higher frequency content creates a response such that the $\mathcal{H}$ fails to contract the solution but still provides a bounded response. This is mostly related to the increased acceleration caused by the higher frequency content at the edges of the cantilever.

4.2. Choosing continuation blending functions

We are choosing a cantilever configuration that is unstable without relaxation for the squared cross-section by applying R=2 and AR=5. The kinematic viscosity is set such that $Re = 5000$, the reason for this choice is to have a reference point typical for transition regime. To capture the differences between different relaxations techniques, we are sampling the displacement in the X direction over a sampling time of 0.8 s. We define the relative difference as the difference divided by the mean value of the absolute value of the reference. As a reference, we are using traction SUR [1 0.8] (21). All solutions have their infinity norm below 10^{-6} which from a threshold study is considered as converged. Note that we do not use the threshold 10^{-8} in this case, instead, we set as we do in the rest of this study, we choose the number of iterations to be fixed such that the infty norm of the residual is less than 10^{-6} for all macro iterations. Otherwise, for some of the relaxations, the error will artificially grow. We choose a stable configuration, then for that given stiffness and mass ratio as initial parameters, we scale the parameters to the desired parameters. We are not including the blending function for damping (ω^d) since this had the least influence on stability, mostly applied

near the stability limit (see below). As blending function Eqn (14) is used and we specify the parameters in the order $[\gamma_0, \gamma_1, \gamma_2]$. For a stable initial configuration without relaxation, we are choosing the following blending functions: (E[1,80,0.6],M[1,5,0.7]). We compare the effect of continuation with IQN-ILS[5] and FIR[12]. The FIR is targeting the second-order vibration [24 Hz] and compression wave [60 Hz] with a cutoff of 12 Hz. IQN-ILS[5] could not reach an FSI tolerance error less than 10^{-7} for all macro steps, this is due to the appearance type II error, which only partly can be remedied by improving the tolerance of convergence for velocity and pressure. However, this issue has been reported elsewhere [45] and we are therefore using these settings in the tolerance for the fluid solver, 10^{-9} for the pressure, and 10^{-9} for the velocity. We are also setting the maximum number of iterations to 21. To achieve a less FSI error than 10^{-6} for FIR, eight iterations was needed. However, for continuation, the blending function has to be sufficiently slow, and by trial and error, the number of precondition iterations is set such that the continuation ends when the blending function reaches 0.998, which is 21 iterations. The relative difference to reference, divided by the norm of the reference is shown in Table 1. The number of fixed iterations are given in parenthesis. From

Relaxation	relative difference (%)
Continuation (21)	-0.26 ± 0.5
IQN-ILS [5](7)	0.17 ± 0.3
FIR [12](8)	-1.2 ± 1.8

Table 1
Comparison study of continuation, IQN-ILS and FIR at Re 5000 using with traction SUR [1 0.8] (21) as reference. The fixed number of iterations is set within parenthesis.

a mesh dependency study, the error for current resolution is around 1% in amplitude response for the first amplitude in force-controlled step case setting. From this, it is clear that equivalence is achieved well within the accuracy of mesh resolution for continuation and IQN-ILS. The cause of the largest difference between the cases is the onset of the cross-flow. This normally starts at about 0.5 s but due to the residues below the threshold, the on-set time may vary. The FIR is applied to the traction, thus filtering away the frequency that can couple with higher structural modes, which eliminates the instability and gives a stable solution. There is an energetic loss by applying FIR, however, the impact on the accuracy is minor. Although the result for continuation and traction SUR are with satisfaction concerning the accuracy, they cost twice as much as IQN-ILS and FIR.

4.3. Stability estimation

The stability of relaxation as a function can be quantified by the maximum mass ratio R for which a stable result is obtained, which we denote as R^*. The purpose of this is to correlate R^* with parameters such as thickness (t), boundary velocity (v) and the stiffness of the cantilever (EI), where I is the second area moment. Also, we seek clarification of when type I and II failure appears.

4.3.1. Case setting and relaxation methods applied

For this purpose, we consider a channel flow case with $Re = 600$ and apply the settings described in section 3 and we vary AR from 5 to 80. To enforce a similar accuracy between each simulation, the time step is therefore changed accordingly except for AR=80, where a slightly larger max Courant number is observed compared to the other cases but still the same on average (∼0.2). The applied relaxation methods procedure is the ones presented in the method section: under-relaxation (SUR), Aitken δ^2 and IQN-ILS[11]. We also include a hybrid technique obtained by simultaneous applying the continuation by using the parametrisation presented in section 4.2 and the IQN-ILS method and then after a preset number of subiterations, the continuation is removed and the end criteria are activated. We denoted this precondition as pIQN-ILS. As for the blending function, we choose an initial configuration with a 0.02 damping ratio and a mass ratio for an initial configuration that is stable for the given cross-section. The damping applied in the continuation is such that it goes to zero and thus not explicit over time, it is only applied during precondition, with the purpose to counteracting the type I, thus allowing lower initial stiffness and/or mass, and by that making the procedure less costly, i.e. fewer precondition steps. But, due to the design of the experiment, the choice of blending function is shown to be irrelevant as long a proper initial configuration is set with a sufficient number of precondition iterations with the appropriate number of previous solution vectors for IQN-ILS.

[11] IQN-ILS-R[X] was applied for AR =5 and X=4,8, the methodology did not improve the stability R^* although a slight improvement in efficiency, increasing with the number of taps (X).

4.3.2. R^* as function of AR

Table 2 shows the value of integer N such that $R^* \simeq 2^N$. As a result, a linear relation with respect to AR will show as a step of one unit between adjacent columns, while cubic relation will give steps of three.

Relaxation \ AR	5	10	20	40	80
None (Implicit)	0	-1	-2	-3	-4
SUR	1	0	-1	-2	-3
Aitken δ^2	5	4	3	1	0
IQN-ILS(4)	4	3	2	0	-1
IQN-ILS(8)	8	5	4	2	1
pIQN-ILS (8)	>16	>16	9	6	2

Table 2
Stability limit$N = log_2(R^*)$ for a channel flow case with ρ_f =1000 at Re = 600.

Table 2 presents the highest integer N for which stable solution is obtained as a function of thickness. For implicit, SUR, Aitkens δ^2 and IQN-ILS, the type I failure is predominant for AR in the range 5 to 80. For IQN-ILS(8) the failure is of type II for AR=5, see next section, but otherwise, mainly of type I. Using pIQN-ILS, we can improve the stability ($AR = 80$) with at least a factor of two. The implied unconditional stability for pIQN-ILS in the first two columns (AR 5 and 10) is fortuitous due to the design of the experiment and the limit in amplitude response for sufficiently large R. Also, by the design of the blending function for pIQN-ILS, the type I failure is not present and the type II failure is suppressed.

Remark on the settings of the R

So far we have kept the fluid density constant and varied the solid density to vary R. Hence, as the limit of the density of the solid goes to zero, the coherent fluid mass moving with the cantilever sets the frequency, which causes the amplitude as well the frequency reaches an asymptotic value. To evaluate the effect, we considered a case with a varying fluid density for a squared cross-section by using IQN-ILS(4). For smaller R, there was a minimal effect on the frequency/amplitude but for larger R they varied linearly with R with no apparent limit in amplitude (increasing) or frequency (decreasing). However, due to the deflection, the flow characteristics change the involving modes in the vibration of the cantilever as well. The R^* in this alternative procedure case is lowered but remains within the margin of precision of the factor of two (R^*=3.5-4). More importantly, as with increasing deflection, type I failure is replaced by type II. This will thus not alter the conclusion made so far in this study regarding R^*, only the way it fails in coupling. Of course, another choice would perhaps be changing the stiffness in such a way as to keep the deflection to the same degree, but that is much undesirable since we aim to show the influence of the boundary velocity on the stability as well.

4.3.3. The role of frequency shift to R^*

The frequency shift due to the added mass effect can be estimated from potential flow theory [39]. As a result, the following expression relates frequency *in vacuo* (f_v) with the FSI frequency (f),

$$f = \left[\frac{1}{1 + R\Gamma}\right]^{\frac{1}{2}} f_v, \tag{15}$$

where $\Gamma = \frac{\pi}{4}\frac{b}{t}$ is the structural form factor. Hence, regarding the frequency shift, with increasing Γ, the greater the shift. In a study [23] of partitioned FSI, for a sufficiently small time step, the stability for SUR/Implicit is limited by structural form factor times the R and is invariant of AR. Although the structural form factors are not the same, different applications and goals and objective, we compute $R^*\Gamma$ and plot against AR by using Table 2, for the result see Figure 6.

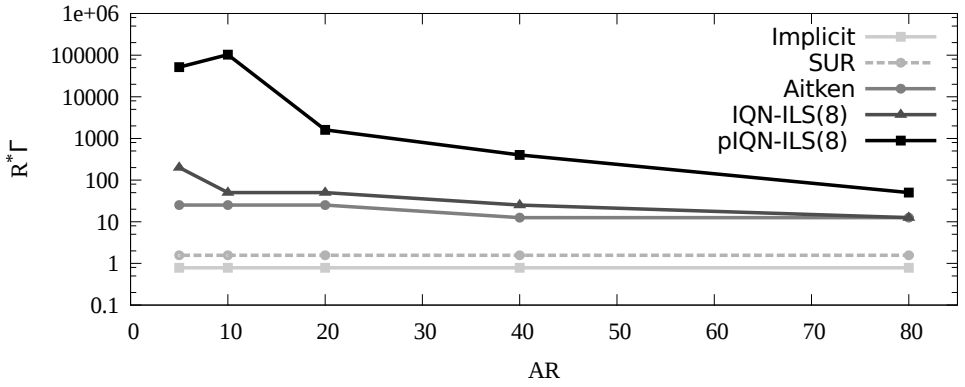

Figure 6: Stability limit (R^*), varying AR between 5 to 80, using Table 2. Increasing stability implies higher shift upwards y axis.

An important result is that all methods except pIQN-ILS have an almost constant $R^*\Gamma$. Higher stability implies a shift upwards along the y-axis. Another interesting feature is that for given R, all relaxation techniques fail for sufficiently large Γ. Further, the norm of the acceleration increases by a factor of 30 in going from AR=5 to AR=80, which is a consequence of the motion control the fluid imposes on the cantilever. The disadvantage with pIQN-ILS is that one needs to know the values of the continuation parameters, however, as it turns out, they are rather insensitive and can be computed at coarser mesh.

For the derived stability, criteria reported elsewhere [21, 28] are using non-dimensional parameters that are difficult to determine for three-dimensional case settings, but from Figure 6, at least for a cantilever case, we can establish that it is enough to compute $R\Gamma$ using Eqn (15) with a known frequency response to obtain is a useful forecast in the design phase. An equivalent measure that connects with the theoretical results is that with increasing added mass, which is for the potential theory $R\Gamma$, the less stable the BGS methodology becomes, which exactly can be concluded from the results presented in Figure 6. However, the crucial difference compared to results presented in the literature is that ours is the very first study that shows empirically the actual improvement the relaxation techniques provide to stability, not efficiency. Most focus on relaxation techniques in the literature has been on efficiency. But the more stable the BGS methodology becomes, the less efficient and more alike the convergence statistics of the relaxation techniques becomes to a point where BGS sometimes is more efficient without relaxation. Further, the closer one reaches each relaxations stability limit, the slower/less efficient the methodology becomes.

4.3.4. The role of boundary velocity and stiffness on R^*

From Figure 6, a linear dependency in R^* with respect to thickness is to be expected, this corresponds to a lowering by 1 between adjacent columns as seen from Table 2. A more refined estimate of R^* for the implicit procedure is performed, for the result see Table 3.

$R^*\backslash$ AR	5	10	20	40	80
Implicit	1.60	0.80	0.44	0.24	0.10

Table 3
Stability limit (R^*) using no relaxation as function of AR.

This establishes the linear dependence of R^* to the thickness. This linearity holds also for SUR. For Aitken δ^2 and IQN-ILS(4), this also applies from AR 5 to 20, but beyond that, the drop suddenly becomes larger. This is most likely due to a gradual change in the compositions of vibrational modes of the cantilever response, which also destabilise the coupling [1, 3]. For the current setting by using beam theory and potential flow theory for the frequency shift, the boundary velocity defined by the mode shape times the phase factor, the shifts between columns in Table 2 lies in the range -1.5 to -2. However, it is observed that this relation does not hold except between the first and second column and instead, the maximum velocity follows a completely different pattern and even decreases for AR =80, see Table

4.

$\lvert v\rvert^*_{max}$ \ AR	5	10	20	40	80
Implicit	0.55	1.67	2.65	3.1	1.97

Table 4
$\lvert v^*\rvert_{max}$ with no relaxation as function of AR. The AR=80 has a significant proportion of an overtone, hence bias the result.

For pIQN-ILS the shift in Table 2 is cubic from AR 20 to 80 due to the absence of type I and type III. This follows by the choice of blending parameters in the continuation method, the stiffness (i.e.EI) is the leading parameter of the stability, using beam theory and with only varying parameter is thickness, hence, by the design of the simulation, the R^* shall then drop by -3 between two adjacent columns for pIQN-ILS. Note that other than pIQN-ILS, type I mask type II failure due to the difference in force response. In conclusion, the type I failure appears to be triggered when the boundary velocity reaches a critical limit thus defining R^*. For all methods except pIQNILS and IQN-ILS with X=8, for AR >5, one need only to compute R^* and thus, unless physical condition changes, R^* can be calculated for only one AR, this is shown in Figure 6.

4.3.5. The influence of mass ratio on type of failure

To illustrate the difference between type I and II failures for IQN-ILS, we are, for a cantilever with AR 5 using IQN-ILS(8) plotting the relative error as a function of subiteration for several values of R, see Figure 7 for the mean and standard deviation of the relative error as function of subiteration index k.

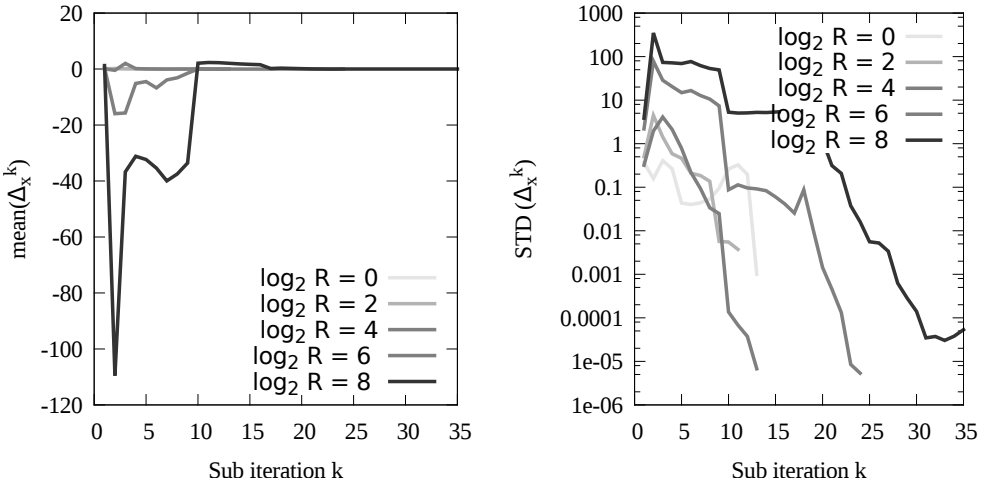

Figure 7: Δ^k in X-direction using IQN-ILS as a function of R for AR = 5. Left Mean value, not the increasing large deviation at the second iteration. Right: Standard deviation of the error, the value increases with increasing R^*.

Although the prediction reduces the relative error, since this is a stiff problem, with a response gain factor of 100, an indication of a type I failure appears after only a few subiterations when operating near R^*. The IQN-ILS successfully suppress the overpressure at the first iterative solution (prediction step), hence reducing the influence of large residuals from the solid step at the mesh moving step where the relaxation is applied, see Figure 7 (left). It should however be emphasised, that two large consecutive residuals with opposite signs, can create an artificial convergence, causing the blending at the third step to become almost zero, and this together with using residuals from the previous time step, which is not applied in this study, the IQN-ILS acts more like a projection method, as was pointed out in [27]. It is therefore important to use the solution of the solid solver as a measure of convergence and to avoid the L^2 norm, the L^∞ norm is more reliable, to suppress local high-frequency residues.

For the current case setting, the limit of the IQN-ILS using taps from the same time step is around X=10. IQN-ILS comes with a cost, some efficiency is lost since the number of intermediate solution steps need to be increased to

maintain stability and somewhat higher-order frequency residues appear in the residual, mostly located at the edges with the highest Courant number. Hence, having a low Courant number often assure good convergence. However, IQN-ILS(4) still has an efficiency comparable to Aitken δ^2. In general, whenever the implicit procedure is stable, the IQN-ILS method is on average slower than Aitkens δ^2. In the region of unstable implicit procedure, the IQN-ILS method often becomes both more stable and more efficient than Aitken δ^2. Also from Figure 7 (right), one can see how the number of iterations required to converge increases with increasing R and there is an indication that the lower limit of Δ^k increases with R, that is the value prior convergence. That limit implies type II failure for sufficiently high R. So although type I is the major cause of divergence, the influence of type II increases with increasing R.

The results in Figure 7 are corroborated by the behaviour of the residual as a function of coupling iteration and mass ratio in [28]. However, as the author of that study observed, it is not feasible to invoke a similar analysis on IQN-ILS as on Aitken δ^2/IGMRES. More importantly, our study shows in more detail the cause of this behaviour. Whenever the coefficient at the third step becomes negative for IQN-ILS, the residual in the next iteration will always increase. A negative value of the coefficient implies a residual with alternation of sign, and to find a solution to this at the solid step, requires higher modes of significant larger frequency, which is a well-known issue in the early investigations of IGMRES.

5. Conclusions

The stability limits for partitioned FSI applied to a three-dimensional case setting of a cantilever immersed in channel flow shows empirically that the SUR and implicit display similar parameter dependency as the theory for linearised and one-dimensional channel flow case with a flexible thin membrane. To determine stability it is sufficient to choose one aspect ratio of the cross-section of the cantilever, then by rescaling the parameter by using beam theory, one obtains the corresponding limits with different cantilever configurations. Further, all relaxation fails for sufficient large frequency shift, implying the added mass term to be the leading term for stability. This is due to the that the structural factor for the theoretical stability shares the same scaling, mass ratio times the ratio of width over thickness, so they behave similarly but with different proportionality constants for stability limits respectively the shift of frequency. As a function of R^*, at instability, we observe that the overpressure is the dominating cause of divergence for SUR and Aitken δ^2, which we denote as type I instability, while IQN-ILS and continuation fail due to growing partition error, which we denote as type II failure. The boundary velocity is the limiting parameter in the fluid solver, which can be related to the incompressible flow condition, while correspondingly the Poisson ratio for the solid solver. While comparing Aitken δ^2 to IQN-ILS, we establish that the Aitken δ^2 method is more efficient than the IQN-ILS while within the stability range of BGS without relaxation, then it gradually becomes less stable until a point where IQN-ILS is more stable and becomes the more efficient. To alleviate the type II failure, there is a strong potential in applying the continuation for a few iterations as a precondition, to suppress the overpressure, that otherwise impairs the stability of the FSI methodology. Also, we identify a feature with IQN-ILS near instability, where the overpressure may suppress the solution to a point it prematurely reaches convergence to the predicted value, requiring the termination step to be at the solid step and removal of the relaxation at the final subiteration, otherwise the IQN-ILS will act as a projection.

Acknowledgement

The computations were enabled by resources provided by the Swedish National Infrastructure for Computing(SNIC) partially funded by the Swedish Research Council through grant agreement no. 2018-05973 and by Lunarc.

Conflict of Interest

Authors have no conflict of interest relevant to this article.

References

[1] Joris Degroote and Jan Vierendeels. Multi-solver algorithms for the partitioned simulation of fluid-structure interaction. *Comput. Methods Appl. Mech. Engrg.*, 200:2195–2210, 2011.

[2] Jan Vierendeels, Lieve Lanoye, Joris Degroote, and Pascal Verdonck. Implicit coupling of partitioned fluid-structure interaction problems with reduced order models. *Computers and Structures*, 85:970–976, 2007.

[3] Joris Degroote, Peter Bruggeman, Robby Haelterman, and Jan Vierendeels. Stability of a coupling technique for partitioned solvers in FSI applications. *Computers and Structures*, 86:2224–2234, 2008.

[4] S. Turek, J. Hron, M. Razzaq, H. Wobker, and M. Schäfer. Numerical benchmarking of fluid-structure interaction: A comparison of different discretization and solution approaches. In Hans-Joachim Bungartz, Miriam Mehl, and Michael Schäfer, editors, *Fluid Structure Interaction II*, volume 73 of *Lecture Notes in Computational Science and Engineering*, pages 413–424. Springer Berlin Heidelberg, 2010.

[5] Matthias Heil. An efficient solver for the fully coupled solution of the large-displacement fluid-structure interaction problems. *Comput. Methods Appl. Mech. Engrg.*, 193:1–23, 2004.

[6] Hermann G. Matthies and Jan Steindorf. Partitioned strong coupling algorithms for fluid-structure interaction. *Computers and Structures*, 81:805–812, 2013.

[7] Ulrich K*ü*ttler and Wolfgang A. Wall. Fixed-point fluid–structure interaction solvers with dynamic relaxation. *Computational Mechanics*, 43(1):61–72, 2008.

[8] Joris Degroote, Klaus-J*ü*rgen Bathe, and Jan Vierendeels. Performance of a new partitioned procedure versus a monolithic procedure in fluid-structure interaction. *Computers and structures*, 87:793–801, 2009.

[9] Jaroslav Hron and Stefan Turek. A monolithic fem/multigrid solver for an ale formulation of fluid-structure interaction with applications in biomechanics. In Hans-Joachim Bungartz and Michael Schäfer, editors, *Fluid-Structure Interaction*, volume 53 of *Lecture Notes in Computational Science and Engineering*, pages 146–170. Springer Berlin Heidelberg, 2006.

[10] C. Michler, S.J. Hulshoff van Brummelen, and R. de Borst. A monolithic approach to fluid-structure interaction. *Computers & Fluids*, 33:839–848, 2004.

[11] Richard L. Muddle, Milan Mihajhović, and Matthias Heil. An efficient preconditioner for monolithically-coupled large displacement fluid-structure interaction problems with pseudo-solid mesh updates. *Journal of Computational Physics*, 231:7315–7334, 2012.

[12] Bj*ö*rn H*ü*bner, Elmar Walhorn, and Dieter Dinkler. A monolithic approach to fluid-structure interaction using space-time finite elements. *Comput. Methods Appl. Mech. Engrg.*, 193:2087–2104, 2004.

[13] Joris Degrootes, Sebastiaan Annerel, and Jan Vierendeels. Stability analysis of gauss-seidel iterations in a partitioned simulation of fluid-structure interaction. *Computers and Structures*, 88:263–271, 2010.

[14] Pongpat Thavornpattanapong, Kelvin Wong, Sherman C.P. Cheung, and Jiyuan Tu. Mathematical analysis of added-mass instability in fluid-structure interaction. *International Journal of Mathematics and Statistics*, 10:43–51, 2011.

[15] Charbel Farhat, Philippe Geuzaine, and Céline Grandmont. The discrete geometric conservation law and the nonlinear stability of ALE schemes for the solution of flow problems on moving grids. *Journal of Computational Physics*, 174(2):669 – 694, 2001.

[16] Jan Nordström and Sofia Eriksson. Fluid structure interaction problems: The necessity of a well posed, stable and accurate formulation. *Communications in Computational Physics*, 8(5):1111–1138, 2010.

[17] M. M. Joosten, W. G. Dettmer, and D. Perić. Analysis of the block gauss–seidel solution procedure for a strongly coupled model problem with reference to fluid–structure interaction. *International Journal for Numerical Methods in Engineering*, 78(7):757–778.

[18] F.J. Profito, D.C. Zachariadis, and D. Dini. Partitioned fluid-structure interaction techniques applied to the mixed-elastohydrodynamic solution of dynamically loaded connecting-rod big-end bearings. *Tribology International*, 140:105767, 2019.

[19] Fabio Nobile and Christian Vergara. Partitioned algorithms for fluid-structure interaction problems in haemodynamics. *Milan Journal of Mathematics*, 80(7):443–467, 2012.

[20] Christopher Winterstein, Andreas andLerch, Kai-Uwe Bletzinger, and Roland Wüchner. Partitioned simulation strategies for fluid–structure–control interaction problems by gauss–seidel formulations. *Advanced Modeling and Simulation in Engineering Sciences*, 5(7):757–778, 2018.

[21] E.H. van Brummelen. Added mass effects of compressible and incompressible flows in fluid-structure interaction. *J. Appl. Mech.*, 76(2):021206, 2009.

[22] P., J.F. Gerbeau, and F. Nobile. Added-mass effect in the design of partitioned algorithms for fluid–structure problems. *Computer Methods in Applied Mechanics and Engineering*, 194(42–44):4506 – 4527, 2005.

[23] Christiane Förster, Wolfgang A Wall, and Ekkehard Ramm. The artificial added mass effect in sequential staggered fluid-structure interaction algorithms. In *ECCOMAS CFD 2006: Proceedings of the European Conference on Computational Fluid Dynamics, Egmond aan Zee, The Netherlands, September 5-8, 2006*. Delft University of Technology; European Community on Computational Methods in Applied Sciences (ECCOMAS), 2006.

[24] C. Conca, A. Osses, and J. Planchard. Added mass and damping in fluid-structure interaction. *Computer Methods in Applied Mechanics and Engineering*, 146(3–4):387 – 405, 1997.

[25] C. Michler, E.H. van Brummelen, and R. de Borst. Error-amplification analysis of subiteration-preconditioned GMRES for fluid-structure interaction. *Comput. Methods Appl. Mech. Engrg.*, 195:2124–2148, 2006.

[26] C. Grandmont, V. Guimet, and Y. Maday. Numerical analysis of some decoupling techniques for the approximation of the unsteady fluid structure interaction. *Mathematical Models and Methods in Applied Sciences*, 11(8):1349–1377, 2001.

[27] Joris Degroote, Robby Haelterman, Sebastiaan Annerel, Peter Bruggeman, and Jan Vierendeels. Performance of partitioned procedures in fluid-structure. *Computers and Structures*, 88:446–457, 2010.

[28] E. H. van Brummelen. Partitioned iterative solution methods for fluid–structure interaction. *International Journal for Numerical Methods in Fluids*, 65(1-3):3–27, 2011.

[29] Emad Tandis and Ali Ashrafizadeh. Numerical simulation of weakly compressible hyper-elastic solids using a conservative pressure-velocity formulation on arbitrary lagrangian-eulerian framework. *Applied Mathematical Modelling*, 96:796–812, 2021.

[30] Saade Adel S. *Elasticity, Theory and Applications*. J. Ross Publishing, 2009.

[31] A. Kalmbach and M. Breuer. Experimental piv/v3v measurements of vortex-induced fluid-structure interaction in turbulent flow - a new benchmark fsi-pfs-2a. *Journal of Fluids and Structures*, 42:369–387, 2013.

[32] Rüdiger Schmidt, Marcus Stoffel, and Thang Duy Vu. Shock tube experiments and Fe-simulation of the structural and material non-linear transient response of plates subjected to blast loading. In *Structures under shock and impact XI : [papers presented at the Eleventh International Conference on Structures under Shock and Impact held in Tallinn, Estonia, July 2010 ; SUSI XI] / ed. N. Jones ...*, volume 113 of *WIT*

Transactions on the Built Environment, pages 207–216, Southampton [u.a.], 2010. WIT Press.

[33] Mitul Luhar and Heidi M. Nepf. Flow-induced reconfiguration of buoyant and flexible aquatic vegetation. *Limnology and Oceanography*, 56(6):2003–2017, 2011.

[34] David Young. Iterative methods for solving partial difference equations of elliptic type. *Transactions of the American Mathematical Society*, 76(1):92–111, 1954.

[35] Johan Lorentzon and Johan Revstedt. A numerical study of partitioned fsi applied to a cantilever in incompressible turbulent flow. *International Journal for Numerical Methods in Engineering*, 121, 10 2019.

[36] Tellervo T Brandt. Study of large eddy simulation and smagorinsky model using explicit filtering. In *36th AIAA Fluid Dynamics Conference and Exhibit*, pages 5–8, 2006.

[37] Hrvoje Jasak, Aleksandar Jemcov, and Zeljko Tukovic. Openfoam: A c++ library for complex physics simulations. 2013.

[38] Klaus-Jürgen Bathe, Ekkehard Ramm, and Edward L Wilson. Finite element formulations for large deformation dynamic analysis. *International Journal for Numerical Methods in Engineering*, 9(2):353–386, 1975.

[39] Wolfgang Bangerth, Ralf Hartmann, and Guido Kanschat. deal. ii—a general-purpose object-oriented finite element library. *ACM Transactions on Mathematical Software (TOMS)*, 33(4):24, 2007.

[40] Hyoungsu Baek and George Em Karniadakis. A convergence study of a new partitioned fluid–structure interaction algorithm based on fictitious mass and damping. *Journal of Computational Physics*, 231(2):629 – 652, 2012.

[41] S.K. Mitra. *Digital Signal Processing: A Computer-based Approach*. McGraw-Hill, 2011.

[42] H Jasak, HG Weller, and AD Gosman. High resolution nvd differencing scheme for arbitrarily unstructured meshes. *International journal for numerical methods in fluids*, 31(2):431–449, 1999.

[43] CF Curtiss and Joseph O Hirschfelder. Integration of stiff equations. *Proceedings of the National Academy of Sciences*, 38(3):235–243, 1952.

[44] D. K. Lilly. A proposed modification of the germano subgrid-scale closure method. *Phys. Fluids*, A(3):633–635, 1992.

[45] R. Haelterman, A.E.J. Bogaers, K. Scheufele, B. Uekermann, and M. Mehl. Improving the performance of the partitioned qn-ils procedure for fluid–structure interaction problems: Filtering. *Computers & Structures*, 171:9 – 17, 2016.